https://doi.org/10.5194/egusphere-2025-4901
Preprint. Discussion started: 22 October 2025

Oxidation-driven acceleration of NPF-to-CCN conversion under polluted atmosphere: Evidence from mountain-top observations in Yangtze River Delta

Weibin Zhu[a,b], Sai Shang[a,b], Jieqi Wang[a,b], Yunfei Wu[a], Zhaoze Deng[a], Liang Ran[a], Ye Kuang[c], Guiqian Tang[a], Xiangpeng Huang[d], Xiaole Pan[a], Lanzhong Liu[e] ,Weiqi Xu[a], Yele Sun[a], Bo Hu[a], Zifang Wang[a], Zirui Liu*[a]

[a] State Key Laboratory of Atmospheric Environment and Extreme Meteorology , Institute of Atmospheric Physics, Chinese Academy of Sciences, Beijing, 100029, China
[b] University of Chinese Academy of Sciences, Beijing, 100049, China
[c] Institute for Environmental and Climate Research, Jinan University, Guangzhou, 511400, China
[d] College of Resources and Environmental Engineering, Jiangsu University of Technology, Changzhou, 213001, China
[e] Shanghuang Atmospheric Boundary Layer and Eco-Environment Observatory, Institute of Atmospheric Physics, Chinese Academy of Sciences, Jinhua, 321203, China

*Corresponding to liuzirui@mail.iap.ac.cn

Abstract: To what extent the new particle formation (NPF) contributed to the CCN remained unclear, especially at the boundary layer top (BLT) in polluted atmosphere. In this study, measurements at a mountain top background site in southeastern China during spring 2024 quantified NPF growth dynamics under different air masses, exploring the nucleation mechanism and its potential contribution to CCN. Eight NPF events were observed, and three of them occurred in the polluted conditions (NPF-P) which associated with regional transportation while the rest five events appeared in the clean conditions (NPF-C). The average formation rate ($J_{2.5}$: 2.4 vs. 0.7 cm^{-3} s^{-1}) and growth rate (GR: 6.8 vs. 5.5 nm h^{-1}) were significantly higher in NPF-P compared to NPF-C, accompany by higher concentrations of sulfuric acid and ammonia, suggesting the important role of ammonia that enhancing sulfuric acid nucleation. In addition, much higher CCN enhancement factor was observed in NPF-P (EF_{CCN}: 1.6 vs. 0.7 in NPF-C) due to the regional transported of anthropogenic pollutants from the urban cluster regions and their secondary transformation under enhanced atmospheric oxidation capacity. Furthermore, the duration of NPF-to-CCN conversion was quantified using "Time Window (τ)", revealing polluted condition accelerated NPF-to-CCN conversion by 17.0% (τ = 16.4 h vs. 19.8 h), with nitrate playing an important role in maintaining rapid GR and compressing τ, thereby enabling clouds to form more readily during NPF days. These findings reveal that polluted air masses enhance both the efficiency and speed of CCN production at the BLT through elevated atmospheric oxidation capacity.

Keywords: New particle formation, Boundary layer top, Pollution condition, Cloud condensation nuclei, Particle growth, Atmospheric oxidation capacity.

1. Introduction

New Particle Formation (NPF) refers to the phenomenon where low-volatility gaseous species form nanoparticles and exhibits rapid bursts in number concentration; these particles may subsequently grow larger through condensation or coagulation (Cai et al., 2024). As an important source of atmospheric particles, NPF profoundly influences cloud microphysical properties, radiative forcing, and precipitation efficiency through its conversion process to Cloud Condensation

https://doi.org/10.5194/egusphere-2025-4901
Preprint. Discussion started: 22 October 2025

Nuclei (CCN), thereby regulating regional and even global climate systems (Kerminen et al., 2018; Machado et al., 2024; Salma et al., 2025; Sun et al., 2025). Growth process of NPF events contributes to generating substantial CCN, with approximately half of CCN in the global troposphere potentially originating from NPF events (Zhao et al., 2024). Under polluted urban atmosphere, NPF event intensity enhanced, with growth processes potentially persisting for 2~3 days and leading to the formation of more particles capable of growing to CCN sizes (Zhang et al., 2019; Zhu et al., 2023). However, the contribution of NPF events to CCN exhibits considerable regional variability, and NPF may even suppress CCN activity under different conditions. However, high condensation sinks (CS) also resulting from higher background particle concentrations strongly suppress nanoparticle formation intensity, accelerate scavenging of small particles, and may reduce particle hygroscopicity, thereby diminishing contribution of NPF to CCN (Salvador et al., 2021). Consequently, substantial uncertainties remain regarding the mechanisms between NPF growth and CCN formation under different atmospheric conditions.

According to abundant field experiment observations, NPF typically manifests as "NPF events" within the global boundary layer; that is, the nucleation of nanoparticles and subsequent growth may occur over horizontal spatial scales extending up to tens or hundreds of kilometers, potentially with significant influence from anthropogenic emissions (Kerminen et al., 2018). Currently, observational research on NPF nucleation and growth processes at the atmospheric boundary layer top (BLT) and their contribution to CCN remains limited, which hinders a full understanding of the nucleation mechanisms underlying NPF. Previous studies have observed variations in CCN number concentration (N_{CCN}) under different supersaturation (SS) and identified influences from factors such as chemical composition (Wu et al., 2024) and seasonal emission differences (Hirshorn et al., 2022). Over the past 30 years, the foundation of experimental observations has been steadily expanded, and numerous computational models have been developed to describe NPF and CCN at mechanistic and empirical levels. Besides, the analysis of process by which newly formed particles grow into CCN was limited. Current research typically quantifies NPF's enhancement of N_{CCN} by comparing N_{CCN} before and after NPF events (denoted as $N_{CCN\text{-}prior}$ and $N_{CCN\text{-}after}$ respectively), using an enhancement factor (EF_{CCN}) generally ranging 0~10 (Liu et al., 2018). Here, $N_{CCN\text{-}prior}$ represents the average N_{CCN} during the two hours preceding an NPF event burst, while $N_{CCN\text{-}after}$ denotes the average N_{CCN} from the onset to the conclusion of NPF's impact on N_{CCN} (Ren et al., 2021; Sun et al., 2021). However, EF_{CCN} only measures quantitative changes in N_{CCN} before and after NPF, failing to reflect the growth speed of small particles to CCN sizes. In polluted atmospheres, high concentrations of anthropogenic pollutants not only significantly affect particle hygroscopic growth capacity but also accelerate condensational growth rate of newly formed particles (Liu et al., 2018). These contrasting findings suggest that precursor abundance, atmospheric oxidation capacity, and background aerosol loading collectively determine whether NPF enhances or suppresses CCN formation. This underscores the need to focus on regions with complex emission mixtures and intense human activity, where both natural and anthropogenic drivers strongly interact.

China has emerged as a critical hotspot for studying NPF-to-CCN processes due to its dense urban clusters and complex interactions between anthropogenic and natural emissions. NPF events

https://doi.org/10.5194/egusphere-2025-4901
Preprint. Discussion started: 22 October 2025

occur frequently in Chinese urban clusters, including the Yangtze River Delta (YRD). Yet, their growth to CCN sizes has rarely been examined, and existing studies are largely restricted to near-surface observations. The YRD area in China, as a globally representative region of intense anthropogenic emissions, provides abundant species for NPF nucleation and growth processes due to its high precursor concentrations (SO_2, NH_3, VOCs, etc.) and active photochemical oxidation processes (generating gaseous sulfuric acid, gaseous nitric acid, and secondary organic aerosols, among others). Notably, the BLT in this region serves as a critical interface connecting polluted air masses with cleaner free tropospheric air, functioning as an "atmospheric reactor". Under these conditions, the mechanisms through which NPF events contribute to CCN at the atmospheric BLT may differ significantly from those in surrounding urban clusters and other high-altitude regions. Studies indicate that high NH_3 concentrations (~10 ppbv; Sun et al., 2023) are frequently observed at this region which promotes an increase in nucleation rates. Simultaneously, organic acids and nitrates generated from VOC oxidation can form low-volatility substances, enhancing particle hygroscopic growth capacity (Huang et al.,2024). However, high precursor concentrations and strong atmospheric oxidation capacity inevitably accompany higher background aerosol concentrations and more complex chemical compositions. Therefore, it is critically important to elucidate how atmosphere with strong atmospheric oxidation capacity under polluted conditions at this BLT environment influence NPF nucleation and growth processes, ultimately determining the efficiency of their contribution to CCN production.

This study conducted comprehensive observations at a high-altitude BLT background site in YRD region in China during spring—a season characterized by frequent NPF events and cloud processes (Qi et al., 2015). By integrating data on particle number size distributions (PNSD, 2 nm~20 μm), aerosol chemical composition, and volatile organic compounds (VOCs) with cluster analysis and model simulations, we focused on investigating the relationship between NPF and cloud condensation nuclei (CCN). Specifically, the study aims to quantify the conversion efficiency from NPF to CCN, identify the mechanisms governing this process under polluted conditions, and propose potential indicators to improve the representation of CCN sources in regional climate models.

2. Methodology

2.1 Experimental site and Instruments

A continuous online observation campaign was conducted at the Shanghuang Ecological and Environmental Observation of the Chinese Academy of Sciences (Shanghuang Station; 28.58°N, 119.51°E) from April 19 to May 30, 2024. The station is located in Jinhua City, Zhejiang Province, at an elevation of 1128 meters above sea level. It is characterized by mountainous terrain and forest coverage, representing a typical high-altitude background environment in the YRD region of China.

Ambient particles and droplets were initially selected using an advanced aerosol–cloud sampling inlet system, which alternated between the PM_1 cyclone, $PM_{2.5}$ cyclone and total suspended particulate (TSP) passage every 20 min (Xu et al., 2024). To minimize particle loss within the sampling system, the relative humidity (RH) at the inlet was maintained below 30% using a Nafion dryer and a sheath air cycle system. Additionally, diffusion and gravitational losses in the

https://doi.org/10.5194/egusphere-2025-4901
Preprint. Discussion started: 22 October 2025

inlet tubing were corrected based on the tubing shape and flow rate (Baron & Willeke, 2001). The particle number size distributions (PNSD) were continuously measured using a system covering the particle size range from 2.5 nm to 16 μm. This system comprises a Neutral cluster and Air Ion Spectrometer (NAIS), a long Scanning Mobility Particle Sizer (long-SMPS, Model 3936, TSI Inc., USA), and an Aerodynamic Particle Sizer (APS, Model 3221, TSI Inc., USA). The time resolution of the PNSD system was set to 5 minutes.

To explore the chemical difference of newly formed particle during their growth processes, the volatile characteristic of those particles was measured using the Thermal Denuder (TD) -SMPS system. Volatile analysis helps distinguish between categories of inorganic compounds, such as nitrates and sulfates and can indirectly provide information on aerosol composition (Schmid et al., 2002). By comparing the volumes of heated (300°C) and unheated particles, the volatility characteristics of particles are studied under the assumption that the particles are spherical and characterized using the volume fraction remaining (VFR) of submicron aerosols. The remaining semi-volatile components are mainly organic compounds, while components such as sulfates and nitrates are evaporated at high temperatures, thereby investigating changes in the proportion of semi-volatile components during the NPF growth process.

The chemical compositions of fine particles—including organics, sulfate, nitrate, ammonium, and chloride, measured using an Aerodyne Time-of-flight aerosol chemical speciation monitor (ToF-ACSM, Li et al., 2023). The instrument sampled ambient air through the same inlet used by the PNSD system, operating at a flow rate of 0.1 L min^{-1}.

Most gaseous species were measured using commercial instruments manufactured by Thermo Scientific (Model Series I). Specifically, SO_2 was measured with a pulsed UV fluorescence analyzer (Model 43i), O_3 with a UV photometric analyzer (Model 49i), and NO_x with a chemiluminescence analyzer (Model 42i). NH_3 was measured using a Picarro G1103 analyzer. All instruments were calibrated prior to the start of the campaign, ensuring consistency and accuracy in the measurements. Additionally, $PM_{2.5}$ mass concentrations were measured using a continuous ambient particulate monitor (Model 5014i, Thermo Scientific, USA), with a $PM_{2.5}$ size cut-off applied prior to the sampling inlet. Calibration of the gas analyzers was performed every two weeks. Meteorological parameters were recorded during the measurement period using an automated weather observation system (Milos520, Vaisala, Finland) positioned adjacent to the PNSD system. A more comprehensive description of the instruments is available in our previous work (Yang et al., 2021).

CCN number concentration can be measured by CCN counter (Model CCN-100; Deng et al., 2011). The instrument operated at five supersaturation —0.07%, 0.11%, 0.20%, 0.40%, and 0.80%—with each level maintained for 15 minutes. To ensure data reliability, measurements were filtered based on established quality control criteria addressing SS instability within the growth chamber (Rejano et al., 2021). The total flow rate was maintained at 0.5 L min^{-1}, with an aerosol to sheath flow ratio of 1:10.

2.2 Data processing of NPF

Typical NPF events were identified based on the classification criteria proposed by Kulmala et al. (2012). An event was defined as NPF only when multiple conditions were simultaneously met, including a distinct burst in nucleation mode particle number concentration and a sustained growth lasting more than two hours. Cases failing to meet these criteria were not classified as NPF events.

https://doi.org/10.5194/egusphere-2025-4901
Preprint. Discussion started: 22 October 2025

The formation rate ($J_{2.5}$), growth rate (GR) and CS were calculated with the commonly used method (Yang et al., 2021). Recognized as a key contributor to particle nucleation, the concentration of sulfuric acid (H_2SO_4) was estimated via a proxy approach proposed by Lu et al. (2019). Additionally, to assess how sulfuric acid (H_2SO_4) influences the early-stage particle growth, its contribution to the initial growth rate was quantitatively evaluated using the equation introduced by Nieminen et al. (2010).

2.3 Calculation of N_{CCN}, activation diameter and hygroscopic parameter

In this study, the N_{CCN} and activation diameter (Da) was calculated by κ-Köhler theory (Petters & Kreidenweis, 2007), which simply link the Da with the supersaturation, is applied as follows, when κ > 0.1:

$$\kappa = \frac{4A^3}{27D_a^3 ln^2 S} \qquad (1)$$

$$A = \frac{4\sigma_\omega M_\omega}{RT\rho_\omega} \qquad (2)$$

Here, σ_ω denotes the surface tension of the droplet at the activation point (σ_ω = 0.072 J·m^{-2}), M_ω is the molecular weight of water (M_ω = 0.018015 kg·mol^{-1}), T is the temperature of the air parcel, R represents the universal gas constant (R = 8.315 J·K^{-1}·mol^{-1}), and ρ_ω refers to the density of water (ρ_ω = 997.1 kg·m^{-3}). The hygroscopicity parameter κ, which reflects the water affinity of aerosols, is influenced by their chemical composition. In this study, κ was estimated using the Zdanovskii–Stokes–Robinson (ZSR) mixing rule (Stokes & Robinson, 1966), based on chemical volume fractions under the assumption of internally mixed particles, following the approach of Gunthe et al. (2011), as follows:

$$\kappa_{chem} = \sum_i \varepsilon_i \kappa_i \qquad (3)$$

Here, κ_i and ε_i represent the hygroscopicity parameter and volume fraction of each individual dry component in the mixture, respectively. The κ values and corresponding densities (ρ) used in the calculations were adopted from Petters & Kreidenweis (2007) and Topping et al. (2005). While the approach combining the critical dry diameter and bulk aerosol properties may introduce some degree of uncertainty, previous studies have shown that the discrepancy between predicted and measured CCN concentrations remains within an acceptable margin of ±20% under both polluted and pristine atmospheric conditions (Zhang et al., 2017).

2.4 Quantification the contribution of NPF to CCN

2.4.1 Enhancement in N_{CCN}

The enhancement in N_{CCN} attributed to NPF events, referred to as EF_{CCN}, was assessed following the methodology described by Kalkavouras et al. (2019) and Ren et al. (2021). The method involves a comparison between the N_{CCN} after and prior to the NPF event:

$$EF_{CCN} = \frac{N_{CCN-after}}{N_{CCN-prior}} \qquad (4)$$

Here, $N_{CCN\text{-}prior}$ represents the two-hour average CCN concentration measured before the onset of the NPF event, while $N_{CCN\text{-}after}$ corresponds to the mean value during the period influenced by the nucleation process. As a simplified approximation, N_{CCN} was estimated by integrating particle

https://doi.org/10.5194/egusphere-2025-4901
Preprint. Discussion started: 22 October 2025

number concentration with a particle size larger than the D_a. The duration over which NPF contributed to CCN was identified by analyzing changes in the time series of N_{CCN} under each applied supersaturation condition. It is important to note that this approach assumes the background level of CCN remains stable throughout the NPF event, thereby neglecting potential influences from alternative aerosol sources or sinks. As a result, the method provides only an approximate evaluation of the NPF impact on N_{CCN}.

2.4.2 Metric to define the duration of NPF to CCN

Beyond the mainstream EF_{CCN} metric, this study proposes an alternative approach that better characterizes NPF hygroscopic growth properties during CCN conversion: using activation diameter (reflecting hygroscopicity of newly formed particles during NPF), onset of NPF at diameter (D_0) and growth rate (GR_{nuc}, describing dynamic size changes). Based on this premise, the metric "Time Window (τ)". This approach more clearly describes the dynamic process where newly formed particles experience hygroscopic growth to become CCN. This study defines the metric "Time Window (τ)" to quantify the time required for newly formed particles to grow from their initial size to CCN-active dimensions. Defined as the duration (hours) required for new particles to grow from initial diameter ($\boldsymbol{D_0}$) to activation diameter, τ is quantified as the time difference between NPF onset and CCN activation diameter:

$$\tau = (D_a - D_0)/GR_{nuc} \qquad (5)$$

where $\boldsymbol{D_a}$ is the average critical activation diameter during NPF events (07:00~18:00 LT), $\boldsymbol{D_0}$ is the average diameter of the smallest nucleation mode particles at NPF onset, $\boldsymbol{GR_{nuc}}$ is the average growth rate throughout the NPF growth phase.

3. Results and Discussion

3.1. Characteristic of NPF events

A typical NPF event are characterized by a sharp increase in the nucleation mode particle number concentration, followed by a sustained increase for more than 2 hours (Dal Maso et al., 2005). According to this standard, eight NPF events were identified across 39 valid observation days from April 19 to May 30 at the Shanghuang station. Note that the number concentration of Nucleation mode particles bursts was also observed on April 30 and May 16 (Figure 1), but these two events were excluded from NPF classification due to the nighttime occurrence without subsequent sustained growth. Meteorological elements (Figure 1e~f) show that southerly winds dominated during the period of observation, with low average wind speeds (1.9 $m \cdot s^{-1}$). The average relative humidity (RH) during the NPF occurrence time (7:00~18:00 LT) was 62.7% and 75.0% for NPF days and non-NPF days, respectively, while the temperature was comparable for NPF and non-NPF days (21.0 and 19.7°C). It is worth noting that NPF2 (May 5) occurred during a cloud interstitial period accompany with high RH (>90%; Figure 1f)with a lower formation rate ($J_{2.5}$=0.8 $nm^{-3}\ s^{-1}$) and a higher growth rate (GR = 5.7 $nm \cdot h^{-1}$). This phenomenon may be attributed to the abundant formation of semi-volatile organic acids via aqueous chemical transformations during the continuous cloud processes, which was previously reported by Kecorius et al. (2023) and they found that a large amount of biogenic terpenoid VOCs (e.g., isoprene) and anthropogenic soluble carbonyl

https://doi.org/10.5194/egusphere-2025-4901
Preprint. Discussion started: 22 October 2025

compounds appeared in cloud water and contributed to the rapid growth of newly formed particle. The data shows that he in-cloud formation of biogenic terpenoid VOCs would be higher during the NFP2 than other NPF-C events(0.3 ppbv vs. 0.2 ppbv). Thus, after cloud dissipation, these compounds would rapidly condense onto the surfaces of small-diameter particles (below 100 nm) under sustained high RH (higher than 90%) and replacing nitrate-dominated growth (NO_3^- fraction lower than 10%), which enabling a large number of particles to continue growing beyond the activation diameter and reach CCN size.

Thus, there was one NPF event in April and seven in May, resulting in an overall NPF frequency of 20.5%. This value is higher than the observational values for European high-altitude sites (900 ~ 1200 meters above sea level) during the springtime (Zugspitze Schneefernerhaus: 3.4%; Hohenpeißenberg: 6.8%; Sun et al., 2024), while it is similar to nearby urban site (Shanghai: 20%; Xiao et al., 2015) and mountain site in North China (Mountain Tai: 21%; Lv et al., 2018). The air mass clustering analysis via backward trajectories (Draxler & Hess, 1998) was performed to track the origination of these NPF events, which identified four distinct air mass categories during the observation period (Figure S1). As showed in Figure S1, Cluster 1 represents the polluted air masses affected by North China Plain urban emissions, Clusters 2 and 4 represent the relative clean air mass affected by western and southern urban emissions, Cluster 3 represents the air masses affected by coastal emissions. Combining trajectory analysis with $PM_{2.5}$ mass concentrations, we categorized the eight NPF events into two types: NPF-C events (occurred under clean conditions in Cluster 2-4) and NPF-P events (occurred under polluted conditions in Cluster 1), with average $PM_{2.5}$ of NPF-P events 100.6 % higher that during NPF-C events (12.8 vs 6.4 $\mu g \cdot m^{-3}$). As showed in Figure 1d, significant variations in 2~6 nm Nucleation mode particles were observed among the eight NPF events, the peak value of which ranged from 246 to 1318 cm^{-3}. The average PNSD during NPF-C events and NPF-P events were fitted as the sum of three mode lognormal distributions (Figure 1a~b, Hussein et al., 2005), and revealed that NPF-P events exhibited higher Aitken mode particle concentrations (3978 cm^{-3}) than NPF-C events (1980 cm^{-3}), while nucleation mode particles (2~6 nm) were lower in NPF-P (575 cm^{-3} vs. 881 cm^{-3}). In addition, the accumulation mode particles were much higher in NPF-P than in NPF-C (881 cm^{-3} vs. 575 cm^{-3}). These results indicate that NPF-P event is primarily influenced by regional transportation, whereas NPF-C reflects the background atmospheric conditions at the BLT of the mountain site.

3.2 Chemical evolution of the NPF-C and NPF-P events

To further explore the chemical difference between NPF-P and NPF-C events, diurnal variation and average values of NPF parameters for NPF-C and NPF-P events were analyzed. As shown in Figure 2a~g, the average formation rate $J_{2.5}$ during NPF-P events (2.5 $cm^{-3}s^{-1}$) tripled that of NPF-C events (0.7 $cm^{-3}s^{-1}$) which close to the values observed at high-altitude sites like Mount Tai (J_3: 1.3 $cm^{-3}s^{-1}$; Shen et al., 2019). This difference is most pronounced at 10:00 local time, when nucleation is relatively strong (2.5 vs. 0.5 $cm^{-3}s^{-1}$). Gaseous sulfuric acid (H_2SO_4) concentrations peaked near noon in both two types of NPF event, with NPF-P events exhibiting an average concentration of 8.2×10^6 cm^{-3}—comparable to European mountainous regions ($7\sim12\times10^6$ cm^{-3}; Gao et al., 2012) and 23.2% higher than NPF-C events. However, compared with the huge difference in

https://doi.org/10.5194/egusphere-2025-4901
Preprint. Discussion started: 22 October 2025

$J_{2.5}$, the difference in gaseous sulfuric acid concentration between the two types of NPF events (23.2%) is insufficient to explain the magnitude of the difference in formation rate. Enhanced NH_3 concentrations during NPF-P events (8.1 ppb vs. 4.1 ppb in NPF-C) may potentially contribute to enhanced nucleation process. Marked difference in O_3 concentrations were recorded, with NPF-P events exhibiting 39.2% higher levels (27.7 ppb) than NPF-C events (19.9 ppb). This difference expanded progressively during the particle growth process (14:00 LT). Consequently, growth rate during NPF-P events exceeded those in NPF-C by 23.6% (6.8 vs. 5.5 $nm \cdot h^{-1}$). Compared with European forested sites (e.g., Hyytiälä, Finland: J_3=0.4 $cm^{-3}s^{-1}$, GR=2.3 $nm \cdot h^{-1}$; Kerminen et al., 2018), the observed J_3 and GR values represent increases of 275% and 126%, respectively, yet remain substantially lower than heavily polluted urban area (1~10 cm^{-3}; Chu et al., 2019). Collectively, the above results indicate that there are significant differences in the intensity of nucleation and growth processes of NPF events under different atmospheric conditions, and these differences are caused by different regional transport processes.

To investigate the chemical differences driving nanoparticle growth during the two types of NPF events, the diurnal variations of chemical components (organics, sulfates, nitrates, ammonia, chlorides, and black carbon) were analyzed during NPF evolution (Figure 2h~i). The results show that during NPF-P events, mass concentrations of all components increased with particle growth, with organics and nitrates exhibiting the most pronounced and sustained increases. In contrast, NPF-C events displayed weaker and less persistent increases in chemical composition concentrations. In both types of NPF events, organics accounted for more than half of the $PM_{2.5}$ mass fraction during the growth stage; however, under the stronger anthropogenic influence in NPF-P events, nitrates played a key role in the later stages of growth, with peak concentrations increasing more than fivefold. Previous field studies in remote regions (Pierce et al., 2012) have also demonstrated that organics are important contributors to new particle growth. Our findings indicate that in anthropogenically influenced mountain regions, nitrates partly substitute for organics in driving NPF growth by exerting strong hygroscopic effects. It should be noted that the analysis was based on $PM_{2.5}$ composition, as the focus was on particle growth to CCN-relevant sizes. Nevertheless, given the size dependence of composition, future studies should incorporate detailed measurements of smaller particle modes.

3.3 Potential formation mechanism of NPF-C and NPF-P events

Gaseous sulfuric acid is recognized as an important specie in nucleation across NPF events. The concentrations during these events ranged from 4×10^6 to 1.2×10^7 cm^{-3}, slightly lower than values reported for urban sites in China (Yao et al., 2018). However, the correlation coefficients R between $J_{2.5}$ and $[H_2SO_4]$ during NPF-C and NPF-P events were 0.77 and 0.87, respectively (Figure 3b), both close to the value reported by Yue et al. (2010) at an urban site of Beijing, where R reached 0.92. This suggests that sulfuric acid was an important proxy for nucleation at this background site. However, this value remains significantly higher than the reported results from clean sites, such as Hyytiälä (Kulmala et al., 2025). Previous studies also proposed that the gaseous species such as ammonia (Kürten et al., 2019) and amines (Metzger et al., 2010) also promote the nucleation.

https://doi.org/10.5194/egusphere-2025-4901
Preprint. Discussion started: 22 October 2025

To explore the potential mechanism of NPF in atmospheric BLT, the relationship between $J_{2.5}$ and [H_2SO_4] in NPF-P and NPF-C were analyzed and compared with those obtained from the CERN-CLOUD experiments, which indicated two kinds of nucleation mechanisms that related to H_2SO_4-NH_3-H_2O nucleation (Kürten et al., 2019) and H_2SO_4-DMA-H_2O nucleation (Almeida et al., 2013). As shown in Figure 3a, solid-colored circles represent three NPF-P events while hollow circles denote five NPF-C events at the Shanghuang station. The range of gas-phase sulfuric acid concentrations corresponding to our measured formation rate falls between those typical of the H_2SO_4–NH_3–H_2O and H_2SO_4–DMA–H_2O mechanisms. However, achieving similar formation rate would require either higher concentrations of DMA or higher levels of NH_3 (Figure 3a). Given the absence of common DMA emission sources in the area (e.g., textile or other industrial activities, Chang et al., 2022), it is more likely that the observed rates are driven by the ambient NH_3 concentration (~5 ppb). Thus, to evaluate the formation mechanism under rich-NH_3 environment, the MALTE-BOX model (Model to predict new Aerosol formation in the Lower TropospherE-BOX) was used to simulate to the formation rate at fixed NH_3 combined with a range of SA concentration. Note that the average atmospheric conditions during the NPF period were used for parameterization (CS = 0.008 s^{-1}, NH_3 concentration = 5 ppb, RH = 66.0%; temperature = 293 K; pressure = 883 hPa).

Figure3b and 3c show the fitted relationships between the product of H_2SO_4 and ammonia concentrations and particle formation rate. The increasing correlation between [H_2SO_4] *[NH_3] and $J_{2.5}$ revealing robust correspondence across both NPF event types. These findings collectively indicate that ternary H_2SO_4-NH_3-H_2O nucleation predominates in NPF at the BLT, irrespective of polluted or clean air mass influences. Consequently, elevated NH_3 concentrations from regional transport significantly contribute to heightened formation rate, complementing the role of sulfuric acid.

3.4. Oxidation-driven acceleration of NPF-to-CCN

To elucidate the relationship between the growth processes of the two types of NPF events and the formation of CCN. N_{CCN} was calculated during the NPF events days using a parameterization method, and the comparison of calculated N_{CCN} with the observed N_{CCN} was conducted. Since supersaturation cannot be measured directly, κ values derived from particle chemical composition and κ-Köhler theory (Bougiatioti et al., 2011), together with prior aircraft measurements of SS (0.1–0.5%; Gong et al., 2023), were used to calculate the critical activation diameter at SS = 0.2%, with local altitude considered. During the growth of NPF events, Da showed significant variability (110.5~128.5 nm), and the average Da for NPF-P events (126.1 nm) exceeded that of NPF-C events (120.0 nm), concomitant with an inversely correlated κ difference (0.18 versus 0.21). According to the chemical composition, organic compounds would be higher in NPF-P events and suppress the condensation processes in ultrafine particles (76.6% vs. 65.4%). It is interesting to note that the average gaseous sulfuric acid and nitric acid concentrations during NPF-P events was much higher than those in NPF-C events, based on the observation data and simulated results using a box model (Figure 2b and Figure S2), which favor to increased condensable vapor precursors, promoting nanoparticle formation. Concurrently, HNO_3 enhances low-volatility organic compound production,

https://doi.org/10.5194/egusphere-2025-4901
Preprint. Discussion started: 22 October 2025

further suppressing the hygroscopicity of NPF-P ultrafine particles. Additionally, Figure 4d reveals a lower semi-volatile compounds fraction in NPF-P events which TD system measurements also corroborate this finding. TD results indicate that NPF-P events contain a higher concentration of non-volatile compounds, which partly contribute to the higher Da.

Figure 4b reveals dynamic coupling behavior between D_a and particle size evolution during NPF processes. During initial nucleation (0~2 hours), elevated non-volatile fractions (Figure 4d) suppress hygroscopic growth, maintaining D_a at higher levels (~120 nm). Diurnal variations in total particle number concentration (N_{CN}) exhibit rapid increases after 07:00 LT, attributable to substantial nanoparticle formation during NPF events. Although cloud condensation nuclei concentrations (N_{CCN}) raise during this process, the CCN activation ratio (AR = N_{CCN}/N_{CN}) declines due to explosive nucleation mode particle production. NPF events demonstrate enhanced N_{CCN} around 09:00 LT—approximately 2 hours after N_{CN} increase. As shown in Figure 4a, the time evolution of D_a across these NPF processes indicate differential CCN activity in newly formed particles under varying atmospheric conditions. Crucially despite the increase in activation diameter, the GR of newly formed particles remains at a high level, and the AR of CCN continues to increase. Consequently, the AR transitions from decline to progressive increase during this period.

The capacity of atmospheric particles to grow into CCN is dominated by multiple factors, including initial particle size and chemical composition (Farmer et al., 2015). Figures 4c~d present variations in chemical composition mass concentrations (organics, nitrate, ammonium, etc.) across eight NPF events, alongside contributions of gaseous sulfuric acid and non-volatile compounds to GR within multiple particle size bins. Figure 4c~d shows that organics components dominate the chemical composition of particles, accounting for an average of over 60%. Within the 14~80 nm particle size bin, the average VFR range from 10% to 20%, which is higher than the observed values under polluted conditions in Beijing (~5%, Wu et al., 2017), suggesting higher degree of oxidation of organics. The contribution of gaseous sulfuric acid to GR diminishes markedly with increasing particle size. For instance, in NPF-C events, its influence declines from ~20% in the 2~6 nm range to < 8% in the 15~20 nm size bin, signifying compounds beyond sulfuric acid substantially drive subsequent nanoparticle growth (Yang et al., 2021; Zhu et al., 2023). The contribution of gaseous sulfuric acid in NPF-P events to GR is consistently lower than in NPF-C counterparts (e.g., 6.1% versus 8.1% in the 9~12 nm bin), suggesting that other substances may contribute to the growth process of particles in polluted condition. Concomitantly, non-volatile volume fraction remaining (1-VFR) demonstrates incremental augmentation with increasing particle diameter (Figure 4d, Δ~5%), approaching 90% within the 60~120 nm size bin. This trend underscores the escalating significance of no-volatile compounds in accelerating nanoparticle growth to CCN sizes as the maturation process proceeds. Notably, the no-volatile VFR is slightly diminished during NPF-P events. This reflects the significant contribution of organic components at the atmospheric BLT and explains why the activation diameter remains at a relatively high level during the initial stage of NPF.

Given the difference in chemical component, the quantification of CCN contributions across

https://doi.org/10.5194/egusphere-2025-4901
Preprint. Discussion started: 22 October 2025

NPF events emerges as important part. To evaluate potential influence of NPF on CCN, CCN enhancement factor (EF_{CCN}) was calculated following methodologies established in previous studies (Kalkavouras et al., 2019; Ren et al., 2021), which characterizes the magnitude of NPF-induced CCN amplification. It emphasizes pre-existing particles, which due to their larger initial diameter, can reach CCN size more quickly and therefore may dominate the CCN enhancement process. As reported by Kalkavouras et al. (2019), pre-existing particles may introduce deviations of up to 50% in estimated CCN enhancements. Given the current challenge in discussing their contributions, EF_{CCN} represents an aggregate outcome encompassing all events. It is showed that EF_{CCN} calculated from N_{CCN} reveals: the NPF-P event on May 28 exhibited the peak value (EF_{CCN}=2.6), whereas the May 17 NPF-C event yielded the minimum value (EF_{CCN}=0.3). The average EF_{CCN} (1.8) for NPF-P events was 160.7% higher than that for NPF-C events (0.7), confirming that precursor enrichment has a significant promoting effect on CCN formation. This is different with other studies that higher EF_{CCN} typically correlates with enhanced anthropogenic influence (Rejano et al., 2021).

However, EF_{CCN} can only reflect the degree of change in CCN concentration before and after NPF events but cannot reflect the dynamics of NPF growth to CCN. This study introduces a novel metric " Time Window (τ)". This parameter characterizes the requisite duration (in hours) for newly formed particles to evolve from initial diameter to activation diameter. Observations reveal substantial τ variability across the eight NPF events (15.1~22.2 h). The average τ value for NPF-P events (16.4 hours) was 17.0% lower than that for NPF-C events (19.8 hours). To present the variation between two NPF event types, diurnal variations of chemical component fraction during NPF events were analyzed (Figure 4e~f). Results indicated that nitrate concentrations in NPF-P events progressively increased during the growth process, particularly after 15:00 LT as particle growth typically persists into nighttime. In contrast, nitrate fraction in NPF-C events remained stable throughout this period. Despite sustained organics dominance (>50% mass fraction), secondary components did not appear to accumulate continuously. Due to lack of no observations of gaseous nitric acid, the F0AM model (Text S1)was used to simulate the concentration of gaseous nitric acid (HNO_3) in these events, showing that its concentration exhibited typical diurnal variation peaks in the afternoon (Figure S2). During particle growth process, HNO_3 concentration averaged 0.60 ppb in NPF-P events—31.4% higher than NPF-C events (0.45 ppb). Although the transported organic compounds promote the formation of more oxidation products (e.g., HOMs), which suppresses the hygroscopic growth of nanoparticles and increases their activation diameter, the enhanced particle formation due to pollution transportation leads to the generation of more CCN once the activation diameter threshold is crossed. Overall, the cross-regional transportation of pollutants fosters stronger nucleation and new particle growth within the boundary layer of the receiving region, thereby further promoting CCN formation. It is worth noting that our $PM_{2.5}$ chemical composition analysis is sufficient to assess growth to CCN-relevant sizes (~120 nm). However, future research should conduct more detailed analyses of smaller particles, as their composition varies with size. A lower τ value driven by strong atmospheric oxidation capacity, accelerates CCN conversion within shorter time—coupling with daytime boundary layer cloud cycles to boost CCN supply efficiency (Kommula et al., 2024). These findings substantiate that enhanced atmospheric oxidation capacity under polluted conditions promotes nitrate formation, thereby accelerating CCN production via NPF

https://doi.org/10.5194/egusphere-2025-4901
Preprint. Discussion started: 22 October 2025

events.

Figure 5a showed the EF_{CCN} (SS=0.2% & 0.4%) against the τ value needed for newly formed particles growth to CCN size across the eight NPF events. This reveals an inverse relationship wherein abbreviated growth durations correlate with heightened NPF contributions to CCN enhancement which means the faster the NPF growth process, the stronger its contribution to CCN. To elucidate the interaction between atmospheric pollution intensity and CCN, the covariation of $PM_{2.5}$ mass concentrations with EF_{CCN}, growth rate, and Time Window (τ) during NPF process (Figure 5b~c) was examined. As shown in Figure 5b, EF_{CCN} exhibits a positive correlation with $PM_{2.5}$ mass concentrations, signifying that elevated precursor concentration maybe enhances NPF growth and intensify nanoparticles conversion to CCN. In all NPF events, Figure 5c shows a clear negative correlation between τ values and growth rate, indicating that regardless of activation state and initial diameter, "GR" promotes the conversion intensity of NPF to CCN. Further analysis reveals a discernible negative correlation between τ value and $PM_{2.5}$ mass concentrations. Additionally, to investigate whether this pattern holds true at other sites, we supplemented multiple sites of different types under the same supersaturation (SS = 0.4%): Leipzig-TROPOS (LTR, 126 m ASL.), Bösel (BOS, 17 m ASL.), Melpitz (MEL, 86 m ASL), Neuglobsow (NEU, 70 m ASL.), Hohenpeißenberg (HPB, 980 m ASL.), Schauinsland (SCH, 1205 m ASL.), and Zugspitze Schneefernerhaus (ZSF, SS = 0.5%, 2670 m ASL.; Sun et al., 2024, Figure 5c). Among these, BOS and LTR are urban background stations, MEL and NEU are regional background stations, and the others are high-altitude background stations. Local $PM_{2.5}$ mass concentrations was calculated by scaling CS from these sites against Shanghuang station's CS due to the absent of reported data. The Time Window (τ) and GR exhibited by these other different types of sites show a significant negative correlation, consistent with the phenomenon observed at Shanghuang station. Under polluted conditions, elevated precursor concentrations (e.g., gaseous sulfuric acid and VOCs) and strong oxidation-driven secondary production during NPF-P events accelerate condensational growth (Hamed et al., 2010). In contrast, reduced gaseous precursors and background particle levels during NPF-C events may hinder nanoparticle growth under relatively clean conditions. Consequently, the accelerated growth kinetics in NPF-P scenarios substantially truncate the τ value required to attain CCN size. Furthermore, in regions that are largely unaffected by anthropogenic emissions, particulate matter growth occurs primarily through self-condensation or condensation deposition processes (Westervelt et al., 2013), resulting in lower N_{CCN} and EF_{CCN} values than those observed in our study. Although some studies have suggested that the conversion of new particles to CCN is suppressed in regions with intensive anthropogenic activity, this conclusion does not hold in background areas affected by pollution transport. In such environments, secondary oxidation products such as HOMs may inhibit the hygroscopic growth of ultrafine particles, but simultaneously, large amounts of transported gaseous precursors (e.g., SO_2 and NO_x) support both the early and subsequent growth of nanoparticles. Through the combined effects of these components, both NPF-C and NPF-P significantly enhanced CCN formation, exhibiting larger growth factors (EF_{CCN}) and faster activation compared with forest background sites abroad.

https://doi.org/10.5194/egusphere-2025-4901
Preprint. Discussion started: 22 October 2025

4. Conclusion

Our intensive mountain-top observations in the YRD demonstrate that polluted air masses substantially accelerate NPF and its conversion to cloud condensation nuclei (CCN). Across eight identified NPF events, those under polluted conditions (NPF-P) exhibited a 360% higher nucleation rate ($J_{2.5}$ = 2.5 vs. 0.7 cm^{-3} s^{-1}) and a 23.6% faster growth rate (GR = 6.8 vs. 5.5 nm h^{-1}) compared with clean events (NPF-C). These enhancements were accompanied by elevated NH_3 concentrations (8.1 vs. 4.1 ppb) and higher gaseous H_2SO_4 (8.2×10^6 cm^{-3}, 23% higher than NPF-C), confirming ternary H_2SO_4–NH_3–H_2O nucleation as the dominant mechanism, consistent with MALTE-BOX simulations. The polluted events further yielded a markedly larger CCN enhancement factor (EF_{CCN} = 1.6 vs. 0.7 in clean cases), reflecting the strong contribution of anthropogenic oxidation products and secondary nitrate condensation. Using the novel "Time Window (τ)" , we show that polluted air masses shortened the NPF–to–CCN conversion timescale by 17.0% (τ = 16.4 h vs. 19.8 h), enabling nascent particles to reach activation sizes within the diurnal cloud cycle. Notably, nitrate accumulation during afternoon growth phases sustained high GR, compressing τ and ensuring efficient CCN supply. These results together suggest that cross-regional pollutant transport enhances precursor abundance, boosts atmospheric oxidation capacity, and accelerates both the magnitude and timing of CCN production at the BLT. In addition, our findings reveal that NPF under polluted conditions may suppress CCN formation, instead showing that in atmospherically oxidizing, transport-influenced regions, pollution intensifies CCN output. Incorporating these oxidation-driven pathways into models is therefore essential for constraining aerosol–cloud–climate feedback in rapidly developing regions.

Author contributions.

ZR and WB designed the experiments, and WB, SS, JQ, YF, ZZ, RL, KY, GQ, XP, XL, LZ, WQ, YL, ZF and HB carried out the field measurements and data analysis. ZR performed the MALTE-BOX model simulation. WB and ZR interpreted the data and wrote the paper. All the authors contributed to discussing results and commenting on the paper.

Competing interests.

The authors declare that they have no known competing financial interests or personal relationships that could have appeared to influence the work reported in this paper.

Financial support.

This work was supported by the Strategic Priority Research Program of the Chinese Academy of Sciences (Grant No. XDB0760200), the National Natural Science Foundation of China [grant numbers 42275120, 42075111, and 42330605] and the National Key Research and Development Program [grant number 2023YFC3706101].

https://doi.org/10.5194/egusphere-2025-4901
Preprint. Discussion started: 22 October 2025

Reference

1 Almeida, J., Schobesberger, S., Kürten, A., Ortega, I. K., Kupiainen-Määttä, O., Praplan, A. P., ... & Kirkby, J. (2013). Molecular understanding of sulphuric acid–amine particle nucleation in the atmosphere. Nature, 502(7471), 359-363.

2 Baron, P. A., & Willeke, K. (2001). Aerosol measurement: principles, techniques, and applications.

3 Bougiatioti, A., Nenes, A., Fountoukis, C., Kalivitis, N., Pandis, S. N., & Mihalopoulos, N. (2011). Size-resolved CCN distributions and activation kinetics of aged continental and marine aerosol. Atmospheric Chemistry and Physics, 11(16), 8791-8808. https://doi.org/10.5194/acp-11-8791-2011.

4 Cai, J., Sulo, J., Gu, Y., Holm, S., Cai, R., Thomas, S., ... & Bianchi, F. (2024). Elucidating the mechanisms of atmospheric new particle formation in the highly polluted Po Valley, Italy. Atmospheric Chemistry and Physics, 24(4), 2423-2441.

5 Chang, Y., Wang, H., Gao, Y., Jing, S., Lu, Y., Lou, S., et al. (2022). Nonagricultural emissions dominate urban atmospheric amines as revealed by mobile measurements. Geophysical Research Letters, 49, e2021GL097640. https://doi.org/10.1029/2021GL097640.

6 Chu, B., Kerminen, V. M., Bianchi, F., Yan, C., Petäjä, T., & Kulmala, M. (2019). Atmospheric new particle formation in China. Atmospheric Chemistry and Physics, 19(1), 115-138.

7 Dal Maso, M., Kulmala, M., Riipinen, I., Wagner, R., Hussein, T., Aalto, P. P., & Lehtinen, K. E. (2005). Formation and growth of fresh atmospheric aerosols: eight years of aerosol size distribution data from SMEAR II, Hyytiälä, Finland. Boreal environment research, 10(5), 323.

8 Deng, Z. Z., Zhao, C. S., Ma, N., Liu, P. F., Ran, L., Xu, W. Y., ... & Wiedensohler, A. (2011). Size-resolved and bulk activation properties of aerosols in the North China Plain. Atmospheric Chemistry and Physics, 11(8), 3835-3846.

9 Draxler, R. R., & Hess, G. D. (1998). An overview of the HYSPLIT_4 modelling system for trajectories. Australian meteorological magazine, 47(4), 295-308.

10 Farmer, D. K., Cappa, C. D., & Kreidenweis, S. M. (2015). Atmospheric processes and their controlling influence on cloud condensation nuclei activity. Chemical Reviews, 115(10), 4199-4217. https://doi.org/10.1021/cr5006292, 2015.

11 Gao, J., Chai, F., Wang, T., Wang, S., & Wang, W. (2012). Particle number size distribution and new particle formation: New characteristics during the special pollution control period in Beijing. Journal of Environmental Sciences, 24(1), 14-21.

12 Gong, X., Wang, Y., Xie, H., Zhang, J., Lu, Z., Wood, R., ... & Wang, J. (2023). Maximum supersaturation in the marine boundary layer clouds over the North Atlantic. AGU advances, 4(6), e2022AV000855. https://doi.org/10.1029/2022AV000855, 2023.

13 Gunthe, S. S., Rose, D., Su, H., Garland, R. M., Achtert, P., Nowak, A., ... & Pöschl, U. (2011). Cloud condensation nuclei (CCN) from fresh and aged air pollution in the megacity region of Beijing. Atmospheric Chemistry and Physics, 11(21), 11023-11039. https://doi.org/10.5194/acp-11-110232011.

14 Hamed, A., Birmili, W., Joutsensaari, J., Mikkonen, S., Asmi, A., Wehner, B., et al. (2010). Changes in the production rate of secondary aerosol particles in Central Europe in view of decreasing SO2 emissions between 1996 and 2006. Atmospheric Chemistry and Physics, 10, 1071–1091. https://doi.org/10.5194/acp-10-1071-2010.

15 Hirshorn, N. S., Zuromski, L. M., Rapp, C., McCubbin, I., Yu, F., & Hallar, A. G. (2022). Seasonal significance

https://doi.org/10.5194/egusphere-2025-4901
Preprint. Discussion started: 22 October 2025

of new particle formation impacts on cloud condensation nuclei at a mountaintop location. Atmospheric Chemistry and Physics Discussions, 2022, 1-26.

16 Huang, H., Xie, X., Xiao, F., Liu, B., Zhang, T., Feng, F., ... & Zhang, C. (2024). A critical review of deep oxidation of gaseous volatile organic compounds via aqueous advanced oxidation processes. Environmental Science & Technology, 58(42), 18456-18473.

17 Hussein, T., Dal Maso, M., Petäjä, T., Koponen, I. K., Paatero, P., Aalto, P. P., ... & Kulmala, M. (2005). Evaluation of an automatic algorithm for fitting the particle number size distributions. Boreal environment research, 10(5), 337.

18 Kalkavouras, P., Bougiatioti, A., Kalivitis, N., Stavroulas, I., Tombrou, M., Nenes, A., & Mihalopoulos, N. (2019). Regional new particle formation as modulators of cloud condensation nuclei and cloud droplet number in the eastern Mediterranean. Atmospheric Chemistry and Physics, 19(9), 6185-6203.

19 Kecorius, S., Hoffmann, E. H., Tilgner, A., Barrientos-Velasco, C., van Pinxteren, M., Zeppenfeld, S., ... & Herrmann, H. (2023). Rapid growth of Aitken-mode particles during Arctic summer by fog chemical processing and its implication. PNAS nexus, 2(5), pgad124.

20 Kerminen, V. M., Chen, X., Vakkari, V., Petäjä, T., Kulmala, M., & Bianchi, F. (2018). Atmospheric new particle formation and growth: review of field observations. Environmental Research Letters, 13(10), 103003. https://doi.org/10.1088/1748-9326/aadf3c, 2018.

21 Kommula, S. M., Buchholz, A., Gramlich, Y., Mielonen, T., Hao, L., Pullinen, I., ... & Virtanen, A. (2024). Effect of long-range transported fire aerosols on cloud condensation nuclei concentrations and cloud properties at high latitudes. Geophysical Research Letters, 51(6), e2023GL107134.

22 Kulmala, M., Petäjä, T., Nieminen, T., Sipilä, M., Manninen, H. E., Lehtipalo, K., ... & Kerminen, V. M. (2012). Measurement of the nucleation of atmospheric aerosol particles. Nature protocols, 7(9), 1651-1667.

23 Kulmala, M., Wei, D., Zhang, X., Zhang, T., Xia, M., Wang, Y., ... & Kokkonen, T. (2025). Understanding atmospheric processes: insights from the comparison between Beijing and Hyytiälä. Npj Clean Air, 1(1), 26.

24 Kürten, A. (2019). New particle formation from sulfuric acid and ammonia: nucleation and growth model based on thermodynamics derived from CLOUD measurements for a wide range of conditions. Atmospheric chemistry and physics, 19(7), 5033-5050.

25 Li, Y., Lei, L., Sun, J., Gao, Y., Wang, P., Wang, S., ... & Sun, Y. (2023). Significant reductions in secondary aerosols after the three-year action plan in Beijing summer. Environmental Science & Technology, 57(42), 15945-15955.

26 Liu, F., Choi, S., Li, C., Fioletov, V. E., McLinden, C. A., Joiner, J., ... & da Silva, A. M. (2018). A new global anthropogenic SO 2 emission inventory for the last decade: a mosaic of satellite-derived and bottom-up emissions. Atmospheric Chemistry and Physics, 18(22), 16571-16586.

27 Liu, P., Song, M., Zhao, T., Gunthe, S. S., Ham, S., He, Y., ... & Martin, S. T. (2018). Resolving the mechanisms of hygroscopic growth and cloud condensation nuclei activity for organic particulate matter. Nature communications, 9(1), 4076.

28 Lu, Y., Yan, C., Fu, Y., Chen, Y., Liu, Y., Yang, G., ... & Wang, L. (2019). A proxy for atmospheric daytime gaseous sulfuric acid concentration in urban Beijing. Atmospheric Chemistry and Physics, 19(3), 1971-1983.

29 Lv, G., Sui, X., Chen, J., Jayaratne, R., & Mellouki, A. (2018). Investigation of new particle formation at the summit of Mt. Tai, China. Atmospheric Chemistry and Physics, 18(3), 2243-2258.

30 Machado, L. A., Unfer, G. R., Brill, S., Hildmann, S., Pöhlker, C., Cheng, Y., ... & Pöschl, U. (2024). Frequent rainfall-induced new particle formation within the canopy in the Amazon rainforest. Nature

https://doi.org/10.5194/egusphere-2025-4901
Preprint. Discussion started: 22 October 2025

Geoscience, 17(12), 1225-1232.

31 Metzger, A., Verheggen, B., Dommen, J., Duplissy, J., Prevot, A. S., Weingartner, E., ... & Baltensperger, U. (2010). Evidence for the role of organics in aerosol particle formation under atmospheric conditions. Proceedings of the National Academy of Sciences, 107(15), 6646-6651.

32 Nieminen, T., Lehtinen, K. E. J., & Kulmala, M. (2010). Sub-10 nm particle growth by vapor condensation–effects of vapor molecule size and particle thermal speed. Atmospheric Chemistry and Physics, 10(20), 9773-9779.

33 Petters, M. D., & Kreidenweis, S. M. (2007). A single parameter representation of hygroscopic growth and cloud condensation nucleus activity. Atmospheric Chemistry and Physics, 7(8), 1961-1971.

34 Pierce, J. R., Leaitch, W. R., Liggio, J., Westervelt, D. M., Wainwright, C. D., Abbatt, J. P. D., et al. (2012). Nucleation and condensational growth to CCN sizes during a sustained pristine biogenic SOA event in a forested mountain valley. Atmospheric Chemistry and Physics, 12, 3147–3163. https://doi.org/10.5194/acp-12-3147-2012.

35 Qi, X. M., Ding, A. J., Nie, W., Petäjä, T., Kerminen, V. M., Herrmann, E., ... & Kulmala, M. (2015). Aerosol size distribution and new particle formation in the western Yangtze River Delta of China: 2 years of measurements at the SORPES station. Atmospheric chemistry and physics, 15(21), 12445-12464.https://doi.org/10.5194/acp-15-12445-2015.

36 Rejano, F., Titos, G., Casquero-Vera, J. A., Lyamani, H., Andrews, E., Sheridan, P., ... & Olmo, F. J. (2021). Activation properties of aerosol particles as cloud condensation nuclei at urban and high-altitude remote sites in southern Europe. Science of the Total Environment, 762, 143100.

37 Ren, J., Chen, L., Fan, T., Liu, J., Jiang, S., & Zhang, F. (2021). The NPF effect on CCN number concentrations: A review and re-evaluation of observations from 35 sites worldwide. Geophysical Research Letters, 48(19), e2021GL095190.

38 Salma, I., Weidinger, T., Rohonczy, J., & Vörösmarty, M. (2025). Types of regional and localised new aerosol particle formation and growth processes: Atmospheric Banana Atlas. npj Climate and Atmospheric Science, 8(1), 261.

39 Salvador, P., Barreiro, M., Gómez-Moreno, F. J., Alonso-Blanco, E., & Artíñano, B. (2021). Synoptic classification of meteorological patterns and their impact on air pollution episodes and new particle formation processes in a south European air basin. Atmospheric Environment, 245, 118016.

40 Schmid, O., Eimer, B., Hagen, D. E., & Whitefield, P. D. (2002). Investigation of volatility method for measuring aqueous sulfuric acid on mixed aerosols. Aerosol Science & Technology, 36(8), 877-889.

41 Shen, L., Wang, H., Yin, Y., Chen, J., & Chen, K. (2019). Observation of atmospheric new particle growth events at the summit of mountain Tai (1534 m) in Central East China. Atmospheric Environment, 201, 148-157.

42 Stokes, R. H., & Robinson, R. A. (1966). Interactions in aqueous nonelectrolyte solutions. I. Solute-solvent equilibria. The Journal of Physical Chemistry, 70(7), 2126-2131. https://doi.org/10.1021/j100879a010, 1966.

43 Sun, J., Hermann, M., Weinhold, K., Merkel, M., Birmili, W., Yang, Y., ... & Wiedensohler, A. (2024). Measurement report: Contribution of atmospheric new particle formation to ultrafine particle concentration, cloud condensation nuclei, and radiative forcing–results from 5-year observations in central Europe. Atmospheric Chemistry and Physics, 24(18), 10667-10687.

44 Sun, J., Hermann, M., Yuan, Y., Birmili, W., Collaud Coen, M., Weinhold, K., ... & Wiedensohler, A. (2021). Long-term trends of black carbon and particle number concentration in the lower free troposphere in Central

https://doi.org/10.5194/egusphere-2025-4901
Preprint. Discussion started: 22 October 2025

Europe. Environmental Sciences Europe, 33(1), 47. https://doi.org/10.1186/s12302-021-00488-w, 2021.

45 Sun, Q., Gu, M., Wu, D., Yang, T., Wang, H., & Pan, Y. (2023). Concurrent measurements of atmospheric ammonia concentrations in the megacities of Beijing and Shanghai by using cavity ring-down spectroscopy. Atmospheric Environment, 307, 119848.

46 Sun, Y., Luo, H., Li, Y., Zhou, W., Xu, W., Fu, P., & Zhao, D. (2025). Atmospheric organic aerosols: online molecular characterization and environmental impacts. npj Climate and Atmospheric Science, 8(1), 305.

47 Topping, D. O., McFiggans, G. B., & Coe, H. (2005). A curved multi-component aerosol hygroscopicity model framework: Part 1–Inorganic compounds. Atmospheric Chemistry and Physics, 5(5), 1205-1222. https://doi.org/10.5194/acp-5-1205-2005, 2005.

48 Westervelt, D. M., Pierce, J. R., Riipinen, I., Trivitayanurak, W., Hamed, A., Kulmala, M., et al. (2013). Formation and growth of nucleated particles into cloud condensation nuclei: Model-measurement comparison. Atmospheric Chemistry and Physics, 13, 7645–7663. https:// doi.org/10.5194/acp-13-7645-2013.

49 Wu, Z. J., Ma, N., Größ, J., Kecorius, S., Lu, K. D., Shang, D. J., ... & Zhang, Y. H. (2017). Thermodynamic properties of nanoparticles during new particle formation events in the atmosphere of North China Plain. Atmospheric research, 188, 55-63.

50 Wu, Z., Wang, H., Yin, Y., Shen, L., Chen, K., Chen, J., ... & Lin, W. (2024). Impacts of the aerosol mixing state and new particle formation on CCN in summer at the summit of Mount Tai (1534m) in Central East China. Science of The Total Environment, 918, 170622.

51 Xiao, S., Wang, M. Y., Yao, L., Kulmala, M., Zhou, B., Yang, X., ... & Wang, L. (2015). Strong atmospheric new particle formation in winter in urban Shanghai, China. Atmospheric Chemistry and Physics, 15(4), 1769-1781.

52 Xu, W., Kuang, Y., Xu, W., Zhang, Z., Luo, B., Zhang, X., ... & Sun, Y. (2024). Hygroscopic growth and activation changed submicron aerosol composition and properties in the North China Plain. Atmospheric Chemistry and Physics, 24(16), 9387-9399.

53 Yang, S., Liu, Z., Clusius, P. S., Liu, Y., Zou, J., Yang, Y., ... & Wang, Y. (2021). Chemistry of new particle formation and growth events during wintertime in suburban area of Beijing: Insights from highly polluted atmosphere. Atmospheric Research, 255, 105553.

54 Yao, L., Garmash, O., Bianchi, F., Zheng, J., Yan, C., Kontkanen, J., ... & Wang, L. (2018). Atmospheric new particle formation from sulfuric acid and amines in a Chinese megacity. Science, 361(6399), 278-281.

55 Yue, D. L., Hu, M., Zhang, R. Y., Wang, Z. B., Zheng, J., Wu, Z. J., ... & Zhu, T. (2010). The roles of sulfuric acid in new particle formation and growth in the mega-city of Beijing. Atmospheric Chemistry and Physics, 10(10), 4953-4960.

56 Zhang, F., Ren, J., Fan, T., Chen, L., Xu, W., Sun, Y., ... & Li, Z. (2019). Significantly enhanced aerosol CCN activity and number concentrations by nucleation-initiated haze events: A case study in urban Beijing. Journal of Geophysical Research: Atmospheres, 124(24), 14102-14113.

57 Zhang, F., Wang, Y., Peng, J., Ren, J., Collins, D., Zhang, R., ... & Li, Z. (2017). Uncertainty in predicting CCN activity of aged and primary aerosols. Journal of Geophysical Research: Atmospheres, 122(21), 11-723. https://doi.org/10.1002/2017jd027058.

58 Zhang, Z., Xu, W., Zhang, Y., Zhou, W., Xu, X., Du, A., ... & Sun, Y. (2024). Measurement report: Impact of cloud processes on secondary organic aerosols at a forested mountain site in southeastern China. Atmospheric Chemistry and Physics, 24(14), 8473-8488.

59 Zhao, B., Donahue, N. M., Zhang, K., Mao, L., Shrivastava, M., Ma, P. L., ... & Wang, L. (2024). Global

https://doi.org/10.5194/egusphere-2025-4901
Preprint. Discussion started: 22 October 2025

variability in atmospheric new particle formation mechanisms. Nature, 631(8019), 98-105.

60 Zhu, W., Hu, B., Liu, Z., Pan, Y., Han, J., Li, C., ... & Wang, Y. (2023). Reduction of anthropogenic emissions enhanced atmospheric new particle formation: Observational evidence during the Beijing 2022 Winter Olympics. Atmospheric Environment, 314, 120094.

https://doi.org/10.5194/egusphere-2025-4901
Preprint. Discussion started: 22 October 2025

Figures

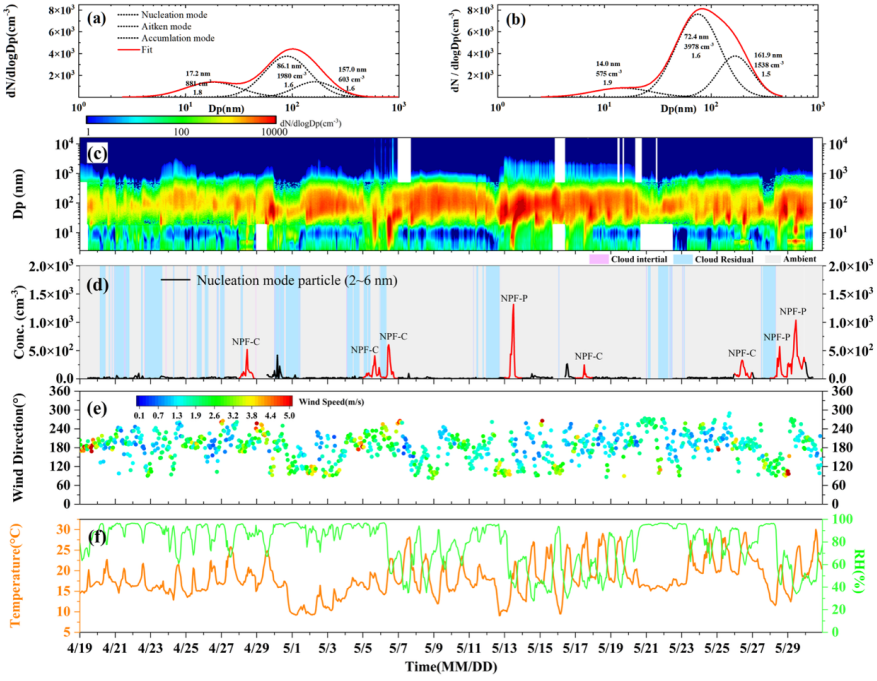

Figure 1. (a~b) Trimodal lognormal fittings for particle number size distributions during NPF-C (clean conditions) and NPF-P (polluted conditions) events. (c) Time series of particle number size distributions (PNSD) during the observation period. (d) Temporal evolution of cloud processes (cloud interstitial, cloud residual, and ambient period) and 2 ~ 6 nm particle concentrations, with red markers indicating NPF days. (e) Wind direction time series, which color intensity scales with wind speed magnitude. (f) Time series of temperature and relative humidity.

https://doi.org/10.5194/egusphere-2025-4901
Preprint. Discussion started: 22 October 2025

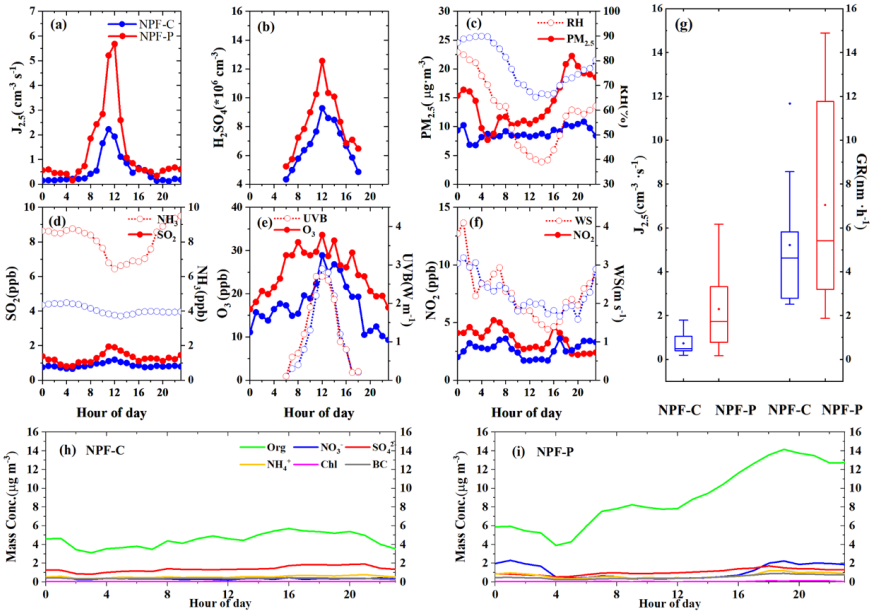

Figure 2. Comparison of diurnal variation species and NPF parameters between NPF-C and NPF-P events. (a) formation rate ($J_{2.5}$); (b) Gaseous sulfuric acid (H_2SO_4) concentration; (c) $PM_{2.5}$ mass concentration and relative humidity (RH); (d) SO_2 and NH_3 concentration; (e) O_3 concentrations and UVB radiation intensity; (f) NO_2 concentration and wind speed; (g) Box plots of formation rate ($J_{2.5}$) and growth rate (GR), where dots represent medians and horizontal lines denote arithmetic means. (h~i) The average diurnal variations of the chemical composition (organic, sulphate, nitrate, ammonium, chlorine and black carbon) during the NPF-C and NPF-P events.

https://doi.org/10.5194/egusphere-2025-4901
Preprint. Discussion started: 22 October 2025

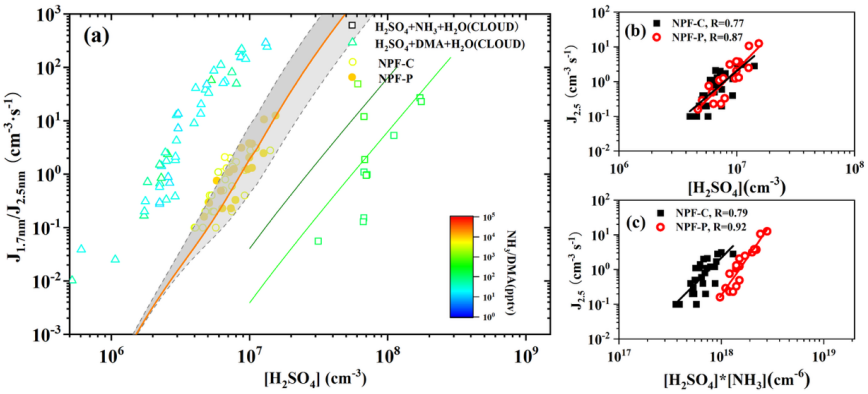

Figure 3. Nucleation mechanism analysis at Shanghuang station. (a) Comparison of observed ($J_{2.5}$), experimental ($J_{1.7}$), and theoretical formation rate versus H_2SO_4 concentration. Field data (colored hollow circles: 5 NPF-C events; solid circles: 3 NPF-P events) are overlaid on CLOUD chamber measurements at 278 K and 38% RH (hollow squares: H_2SO_4-NH_3-H_2O ternary nucleation at NH_3 = 0.1 ppbv & 1 ppb; triangles: H_2SO_4-DMA-H_2O ion-mediated nucleation at DMA = 13~140 pptv) (Kürten et al., 2019; Almeida et al., 2013). Color scales in (a) denote NH_3 (blue gradient) and DMA (red gradient) mixing ratios. MALTE-BOX model prediction shows H_2SO_4 nucleation with 5 pptv NH_3 (yellow line) ± binding energy uncertainty (gray band, ±1 kcal·mol^{-1}). (b) Formation rate ($J_{2.5}$) versus [H_2SO_4] for NPF-C (black squares) and NPF-P (red hollow circles) events. (c) Formation rate ($J_{2.5}$) versus [H_2SO_4] × [NH_3] product, with Pearson correlation coefficients (R).

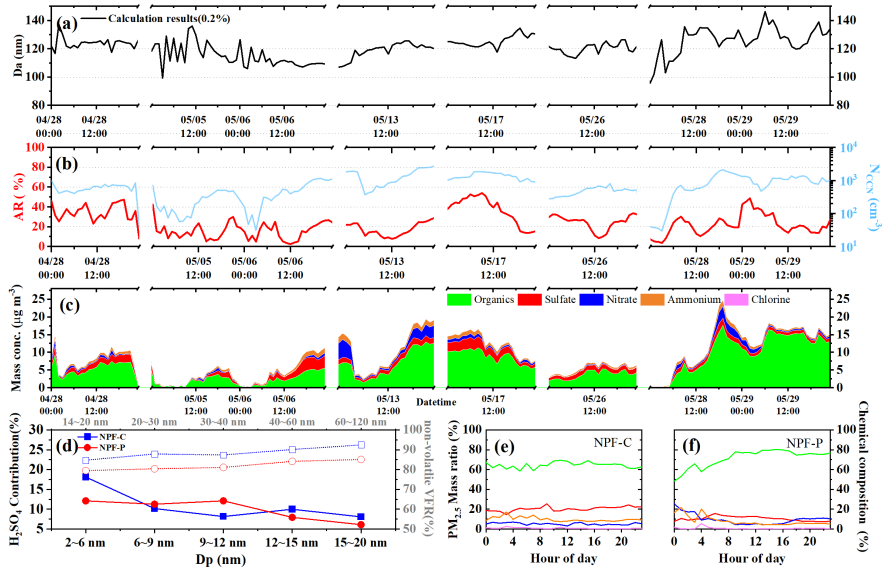

Figure 4. CCN-related parameters and chemical compositions across all NPF events. (a) Black solid line denotes calculated activation diameter for eight NPF events (SS=0.2%). (b) Temporal evolution of N_{CCN} (blue solid line) and its activation ratio (AR = N_{CCN}/N_{CN}, red solid line). (c) Time-resolved mass concentrations of particulate chemical constituents (organics, nitrate,

https://doi.org/10.5194/egusphere-2025-4901
Preprint. Discussion started: 22 October 2025

ammonium, etc.) during the eight NPF events. (d) Solid line represents the fractional contribution of gaseous sulfuric acid to growth rate (GR) within 2 ~ 20 nm particles; dashed line represents the non-volatile volume fraction remaining (1-VFR) in the 14 ~ 120 nm size bin. (e~f) Diurnal variations in mass fraction contributions of chemical constituents during NPF-C (clean) and NPF-P (polluted) events, respectively.

https://doi.org/10.5194/egusphere-2025-4901
Preprint. Discussion started: 22 October 2025

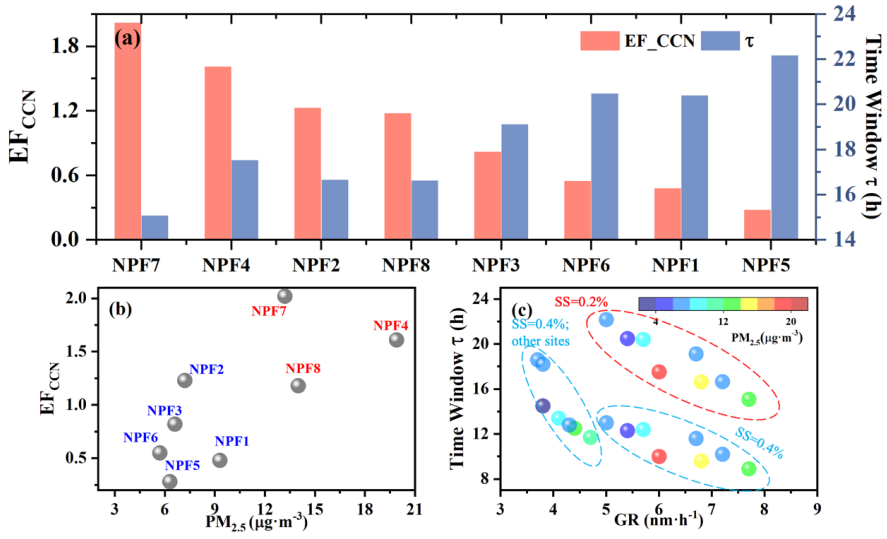

Figure 5. Scatter distributions illustrating relationships among CCN enhancement factor (EF_{CCN}), τ value for particle growth to CCN size, and associated parameters. (a) EF_{CCN} versus τ across eight distinct NPF events; (b) Correlation analysis between $PM_{2.5}$ mass concentrations and EF_{CCN}; (c) Relationship between GR and τ value—color gradient denotes $PM_{2.5}$ mass concentration in Shanghuang station(SS=0.2% & 0.4%) and other sites (SS=0.4%).